Materials and Design 195 (2020) 109006

Contents lists available at ScienceDirect

Materials and Design

journal homepage: www.elsevier.com/locate/matdes

Removal of ammonium from wastewater with geopolymer sorbents fabricated via additive manufacturing

Giorgia Franchin [a], Janne Pesonen [b], Tero Luukkonen [c,*], Chengying Bai [d], Paolo Scanferla [a], Renata Botti [a], Sara Carturan [e], Murilo Innocentini [f], Paolo Colombo [a,g]

[a] Department of Industrial Engineering, University of Padova, Via Marzolo 9, 35131 Padova, Italy
[b] Research Unit of Sustainable Chemistry, University of Oulu, P.O. Box 8000, 90014 Oulu, Finland
[c] Fibre and Particle Engineering Research Unit, University of Oulu, P.O. Box 8000, 90014 Oulu, Finland
[d] Key Laboratory of Superlight Materials and Surface Technology, Ministry of Education, College of Materials Science and Chemical Engineering, Harbin Engineering University, 150001 Harbin, China
[e] Legnaro National Lab, National Institute for Nuclear Physiscs (INFN), Viale dell'Università 2, 35020 Legnaro, Italy
[f] Course of Chemical Engineering, University of Ribeirão Preto (UNAERP), 14096-900 Ribeirão Preto, São Paulo, Brazil
[g] Department of Materials Science and Engineering, The Pennsylvania State University, University Park, State College, PA 16802, USA

HIGHLIGHTS

- Geopolymer sorbents were prepared via Direct Ink Writing (DIW).
- The synergy between material and fabrication provides optimal porosity.
- Proof-of-concept study of aqueous NH_4^+ removal with 3D-printed geopolymers.
- High permeability, high cation exchange capacity, and reusable for multiple times.

GRAPHICAL ABSTRACT

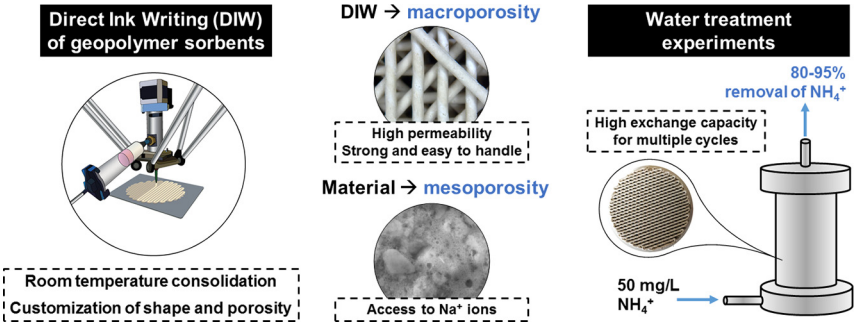

ARTICLE INFO

Article history:
Received 24 March 2020
Received in revised form 24 June 2020
Accepted 25 July 2020
Available online 28 July 2020

Keywords:
Geopolymer
Additive manufacturing
Direct ink writing
Nitrogen
Ammonium removal
Wastewater

ABSTRACT

Geopolymers have been recently explored as sorbents for wastewater treatment, thanks to their mechanical and chemical stability and to their low-energy manufacturing process. One specific application could be the removal of ammonium (NH_4^+) through exchange with Na^+ ions. Additive manufacturing (AM) represents an especially interesting option for fabrication, as it allows to tailor the size, distribution, shape, and interconnectivity of pores, and therefore the access to charge-bearing sites. The present study provides a proof of concept for NH_4^+ removal from wastewater using porous geopolymer components fabricated via direct ink writing (DIW) AM approach. A metakaolin-based ink was employed for the fabrication of a log-pile structure with 45° rotation between layers, producing continuous yet tortuous macropores which are responsible for the high permeability of the sorbents. The ink consolidates in an amorphous, mesoporous network, with the mesopores acting as preferential sites for ion exchange. The printed sorbents were characterized for their physicochemical and mechanical properties and the NH_4^+ removal capacity in continuous-flow column experiments by using a model effluent. The lattices present high permeability and high cation exchange capacity and maintained a high amount of active ions after four cycles, allowing to reuse them multiple times.

* Corresponding author at: Fibre and Particle Engineering Research Unit, University of Oulu, P.O. Box 8000, 90014 Oulu, Finland.
E-mail address: tero.luukkonen@oulu.fi (T. Luukkonen).

https://doi.org/10.1016/j.matdes.2020.109006

1. Introduction

Geopolymers (amorphous aluminosilicates) are versatile materials, which have attracted attention in many environmental applications. In water and wastewater treatment, they have been studied as adsorbents or ion exchangers [1–9], photocatalysts [10,11], membrane materials [12,13], pH adjustment agents [14–18], and for the solidification/stabilization of water treatment residues [19], to name just a few examples. Main drivers for this emerging interest are their good mechanical and chemical stability coupled with a relatively simple and low-energy manufacturing process [20]. Consequently, geopolymers could offer feasible options for competing materials in water treatment such as synthetic zeolites, conventional ceramics, or polymeric components in terms of costs, environmental impacts, and performance.

One specific use for geopolymers could be the removal of ammonium (NH_4^+) from wastewaters [21–23]. Legislative requirements for nitrogen removal from municipal and industrial wastewaters are becoming increasingly common to prevent eutrophication. In fact, ammonium is the nitrogen species with the largest contribution to the eutrophication in water bodies where nitrogen is the nutrient in shortest supply [24]. Conventional methods for nitrogen removal are based on the microbial nitrification-denitrification, which can be ineffective at low temperatures [25] and have higher operational costs in comparison to ion exchange-based process [26]. Geopolymers have a high affinity for NH_4^+: the charge-balancing Na^+ cations in the geopolymer aluminosilicate network may be exchanged to NH_4^+ up to near 100% efficiency [27]. However, it is required that the charge-bearing sites are accessible. The reported ion exchange capacities of powdered metakaolin geopolymer for NH_4^+ have been 18–32 mg g^{-1} [22], depending on the tested water matrix (raw wastewater after screening or after advanced primary treatment), which are comparable to many natural or synthetic zeolites [21]. Moreover, geopolymer granules were tested for ammonium removal on a bench-scale column experiment taking place at a wastewater treatment plant: < 4 mg/ L NH_4^+ was consistently reached at water temperature of 10 °C (usually 12 °C is the limit for an efficient operation of nitrification-denitrification process), and the material could be regenerated with NaCl/NaOH [22].

The development of geopolymer sorbents requires also considerations for how to apply them in practice. It is possible to dose powdered sorbent continuously, but then an additional process phase is required to separate the used sorbent and operational costs can become high. Consequently, various options to prepare permeable and highly porous geopolymers have been developed: for instance, direct foaming, freeze casting, sacrificial template method, granulation, or additive manufacturing (AM) [20].

AM refers to a family of technologies in which a part is directly generated from a virtual model by the addition of material (instead of subtraction or formation), usually in a layer-by-layer approach [28]. Consequently, it is possible to generate parts with variable, complex geometries without the need of adapting the typical manufacturing process itself. The processing requirements (in terms of feedstock and/or sintering), however, can be very challenging, particularly for ceramic materials [29]. Proof of concept for powder based AM of geopolymers was for the first time demonstrated in the literature with a mixture of sand, slag and solid sodium silicate, and an aqueous binder (water and 2-pyrrolidone) [30]; parts produced with this approach, however, possessed high residual porosity (~60%$_{vol}$) and low mechanical properties (compressive strength <1 MPa), as the reaction was not completed.

On the other hand, sol-gel like network formation in geopolymer slurries provides them with a rheological behavior which is consistent with the requirements of the family of extrusion based AM processes, such as direct ink writing (DIW) [31]. Also known as robocasting, the process is based on the extrusion of a ceramic paste (ink) in the form of a filament and its deposition on a substrate following a virtual model. The ink should show an initial yield stress and have a viscosity which decreases with increasing the shear rate (Herschel-Bulkley fluid). Geopolymer slurries possess intrinsic shear thinning behavior, but the geopolymer reaction should be controlled in order to achieve a suitably large temporal printing window; additional tuning of their rheology with organic or inorganic additives allows to fabricate complex structures and lattices with spanning, unsupported features [32–34]. However, research has been mainly focusing on construction applications and therefore large scale extrusion systems, with nozzle diameter up to 20 mm [35–37].

DIW represents an especially interesting option for preparing sorbents, as it allows to precisely control the pore size, size distribution, shape, and interconnectivity, with a resolution of few hundred micrometers [38]. Moreover, topological optimization would enable the fabrication of components with an optimal combination of properties, such as low pressure drop, sufficient strength and contact time.

Consequently, the objective of the present study was to evaluate the performance of porous geopolymer components fabricated via DIW for the removal of NH_4^+ ions in continuous flow of a model wastewater. A metakaolin-based geopolymer ink was employed for the fabrication of a specifically designed log-pile structure with 45° rotation between layers. The mix design was based on fabrication process requirements, in particular achieving a precise control of the slurry rheology and reactivity [32]. The printed components were characterized for their physicochemical and mechanical properties, permeability and NH_4^+ removal capacity. The regenerability of the spent geopolymer components was also assessed.

2. Experimental section

A Na-based geopolymer was prepared by mixing metakaolin (Argical 1200S, Imerys S.A.) as an aluminosilicate source, and an alkaline solution of sodium silicate (SS2942, Ingessil S.r.l.), sodium hydroxide (NaOH, Sigma–Aldrich) and distilled water. The alkaline solution had a molar ratio of $SiO_2/Na_2O = 1.4$ and solids content of 38.5%$_{wt}$. The molar ratios of the geopolymer were: $SiO_2/Al_2O_3 = 3.8$, $Na_2O/Al_2O_3 = 1$ and $H_2O/Al_2O_3 = 13$. Polyethylene glycol with an average molecular weight of 1000 g/mol (PEG 1000, Sigma-Aldrich) was added to the ink (5%$_{wt}$) as a rheological additive. The complete procedure is described in a previous work and reported in the Supplementary Information [32]. The prepared ink had an optimized Bingham pseudoplastic behavior, enabling the fabrication of components with suspended features (struts).

The ink was fed to the DIW device (Delta Wasp 2040 Turbo, Wasproject) by a pressurized vessel, with a typical pressure of $1{\cdot}10^5$ Pa to $5{\cdot}10^5$ Pa; a screw extruder forced the ink through the tip of a conical nozzle with a diameter of 840 μm (Nordson Italia S.p.A.). The printer was configured with a print speed of 10 mm/s and extrusion flow as needed to obtain constant writing. The process was carried out at room temperature and in air. After printing the first layer, the nozzle was raised by 600 μm in the z-direction to print the next layer, providing greater contact between the layers coming from that overlay between them. The first layer was composed of filaments parallel to each other, while the second layer was comprised of parallel filaments but with a rotation of 45° from the previous layer; the subsequent layers followed the same arrangement. The printing process was repeated for 16 layers until the final dimensions of the lattice were reached. Following this pattern, cylindrical sorbents with 45.8 mm diameter and 9.6 mm height were produced. For porosity and mechanical characterization purposes, parallelepipeds with a 15 mm × 15 mm base and 9.6 mm height were produced with the same pattern and designed porosity as the sorbents. The printed samples were placed in the oven at 75 °C for 2 days in a closed box to accelerate the geopolymerization reaction [39]; they were then stored at room temperature for 1 month before characterization and use.

Part of the samples was also washed in continuous flow of deionized water with a flow rate of 1.0 L/h for 8 h. This step mimicked the washing

procedure performed on the sorbents before performing the adsorption tests. Part of the cured and of the washed samples was also ground to fine powders for X-ray diffraction, helium pycnometry and Fourier transform infrared spectroscopy.

A slurry of the same geopolymer composition was produced using the same materials and procedure but excluding the addition of PEG; it was casted, cured at 75 °C for 2 days in a closed mold and then ground into a fine powder for measuring N_2 gas adsorption-desorption isotherms.

Macroscopic evaluation of the structures was performed by means of an optical stereomicroscope (STEMI 2000-C, Carl Zeiss AG) on the printed structures.

The microstructure was assessed by means of a field emission scanning electron microscope (Sigma FESEM, Carl Zeiss AG) on the as prepared printed structures. Secondary electron (SE) images were obtained at accelerating voltage of 5 kV.

The crystalline phase assemblage was investigated by X-ray diffraction (XRD, Bruker AXS-D8 advance) with CuK_α radiation at 40 kV and 40 mA on metakaolin and on powders obtained by grinding printed structures. Data were collected in the range of 10–70° 2θ with a scanning step of 0.05° and a scanning time of 1 s/step. A semi-automatic phase identification was provided by the Match! software package (Crystal Impact GbR), supported by data from the Crystallography Open Database (COD [40]).

The bulk density of the parallelepiped components was evaluated from mass and volume measurements. The apparent and true density values were measured using a helium gas pycnometer (AccuPyc 1330, Micromeritics) on fragments of the printed structures and on finely ground powders, respectively. Using these density values, the closed and open porosity were evaluated, and the latter compared with the theoretical porosity of the CAD file (calculated modeling the struts as dense cylinders).

The compressive strength was measured at ambient conditions with a universal testing machine Instron 1121 UTM (Instron Danvers) under a deformation controlled loading rate of 0.5 mm/min; the value is reported as mean ± standard deviation of at least 8 samples.

The specific surface area (SSA) was determined using N_2 gas adsorption-desorption isotherms at −196 °C (ASAP 2020, Micromeritics and Quantachrome Autosorb iQ, Anton Paar GmbH). SSA was calculated based on the Brunauer, Emmett, Teller (BET) isotherms; average pore widths were calculated from desorption data using the Barrett–Joyner–Halenda (BJH) method. Prior to the analysis, the samples were degassed at 120 °C for approximately 15 h under reduced pressure. The measurement was performed on three kinds of specimens: 1) fragments of the printed structures; 2) fragments of the printed structures after washing; 3) powders from ground PEG-free casts. The results are reported with an estimated experimental error of ±5% (with a minimum error of ±0.5 m^2/g).

Infrared spectra were obtained by ATR - FTIR spectroscopy (6200 FTIR spectrometer equipped with ATR Pro One diamond prism, Jasco Inc.). Absorption spectra were determined for fine powders from printed structures before and after washing procedure on 4000–500 cm^{-1} range; they are reported in the Supplementary Information.

Permeability measurements were performed using a laboratory-made apparatus; details of the setup are described in the Supplementary Information. Tests were performed in steady-state regime with dry airflow at room conditions (T ~ 25 °C and $P_0 = P_{atm}$ ~ 1 bar). The test sample was sealed within a cylindrical sample holder with a circular flow area (A_{flow}) of 172 mm^2. The pressure gradient across the specimen was measured by a digital manometer (Sper Scientific 840,083), in response to variations in the air volumetric flow rate Q controlled by a needle valve and measured with a rotameter open to the atmosphere. Flow rate (Q) was corrected to the value at sample exit (Q_0) and finally converted to superficial velocity by $v_s = Q_0/A_{flow}$.

The collected data set (ΔP and v_s) for each test was fitted according to Forchheimer's equation, which expresses the experimental relationship between the fluid pressure applied through a porous medium (ΔP) and the resulting superficial fluid velocity (v_s) permeated through the medium [41]:

$$\frac{\Delta P}{L} = \frac{\mu}{k_1} v_s + \frac{\rho}{k_2} {v_s}^2 \tag{1}$$

in which L is the medium length or thickness along the macroscopic flow direction, and μ and ρ are respectively the viscosity and density of the fluid (for a dry airflow at room conditions: $\mu = 1.84 \cdot 10^{-5}$ Pa·s and $\rho = 1.18$ kg/m^3).

The parameters k_1 and k_2 are respectively known as Darcian and non-Darcian permeability coefficients. These coefficients are only dependent on the porous structure and weigh the contributions of viscous and inertial losses on the total pressure drop. The fitted k_1 and k_2 values were used to predict the pressure drop in the column for water flow in the ion exchange tests.

NH_4^+ ion exchange experiments for the printed components were conducted as continuous flow-through experiments at room temperature (20 ± 1 °C). A model solution (NH_4^+ = 50 mg/L) was prepared by dissolving NH_4Cl (Merck Group) into de-ionized water. A column with an inner diameter of D = 44 mm and height h = 99 mm was filled with a stack of 11 printed sorbents. Sorbent bed was first washed with a continuous flow of de-ionized water (8 L, with a flow rate of 1.0 L/h) in order to decrease the pH down to ~7 and to flush any raw material residues (e.g., PEG 1000). Ammonium solution was then pumped through the bed at a flow rate of 0.5 L/h, corresponding to ~19.3 min empty bed contact time and 0.33 m/h surface loading rate. After filtration, the bed was flushed again with 8 L of de-ionized water. The experiment was repeated 4 times on the same stack; the 1st and 2nd cycles were conducted at a flow rate of 0.5 L/h, whereas the 3rd and 4th cycles were conducted at twice the initial flow rate (1.0 L/h), corresponding to ~9.6 min empty bed contact time and 0.66 m/h surface loading rates. Two different flow rates were tested in order to evaluate the effect of different contact times. The sorbent bed was regenerated between each cycle by pumping 2 L of 0.1 M sodium hydroxide (Merck Group) and 0.2 M sodium chloride (J.T. Baker) solution through the bed at a rate of 2 L/h and rinsing with 8 L of de-ionized water. NH_4^+ concentration was measured with the use of a NH_4^+-selective electrode (Intellical ISENH4181, Hach) connected to a portable multi meter (HQ40d, Hach).

Mass transfer resistance in the column experiments was assessed according to the method described by Fulazzaky et al. [42] In short, the internal ($[k_La]_d$), external ($[k_La]_f$), and global ($[k_La]_g$) mass transfer coefficients (1/h) were determined with Eqs. (2)–(4), respectively. These variables were then plotted against the percentage of outflow from the column and the curves were used to determine whether the mass transfer resistance is dependent on internal or external diffusion.

$$[k_La]_d = [k_La]_g - [k_La]_f \tag{2}$$

$$[k_La]_g = e^{B\beta + \ln(\ln(C_0/C_t))} \tag{3}$$

$$[k_La]_f = [k_La]_g \cdot e^{-\beta \cdot \ln q_c} \tag{4}$$

where B (mg g^{-1}) is potential mass transfer index relating to the driving force of mass transfer, β [(gh)/mg] is sorbate-sorbent affinity parameter, C_0 (mg/L) and C_t (mg/L) are initial NH_4^+ concentration and concentration at time t (h), respectively and q_c (mg g^{-1}) is the cumulative adsorbed amount of NH_4^+ on the sorbents. B and β were determined from the intercept and slope, respectively, by plotting ln q_c versus ln t according to Eq. (5).

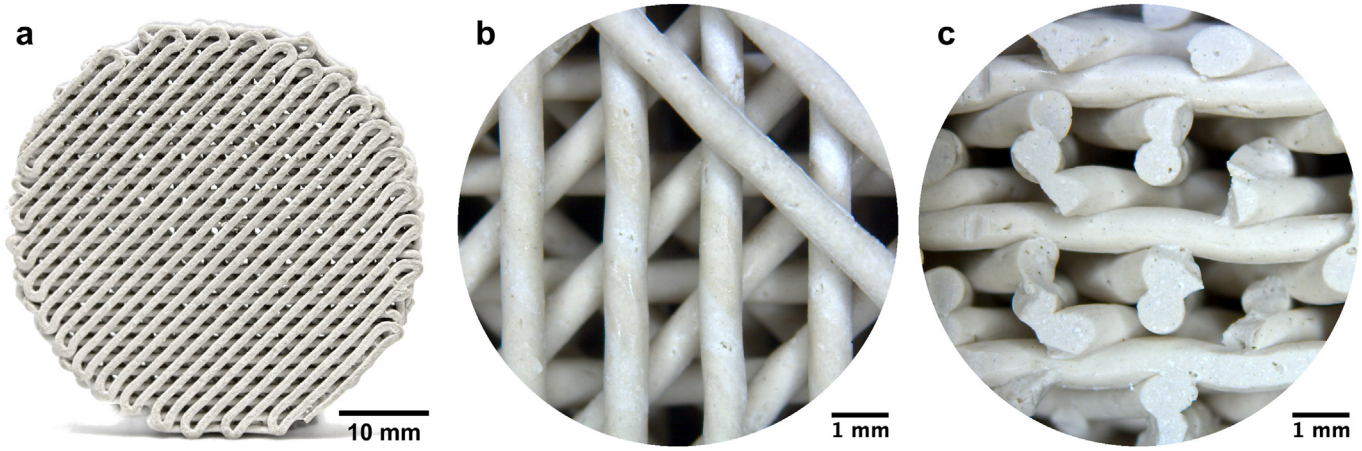

Fig. 1. Cylindrical sorbent produced by DIW: a) overview, b) top view and c) section side view at higher magnification.

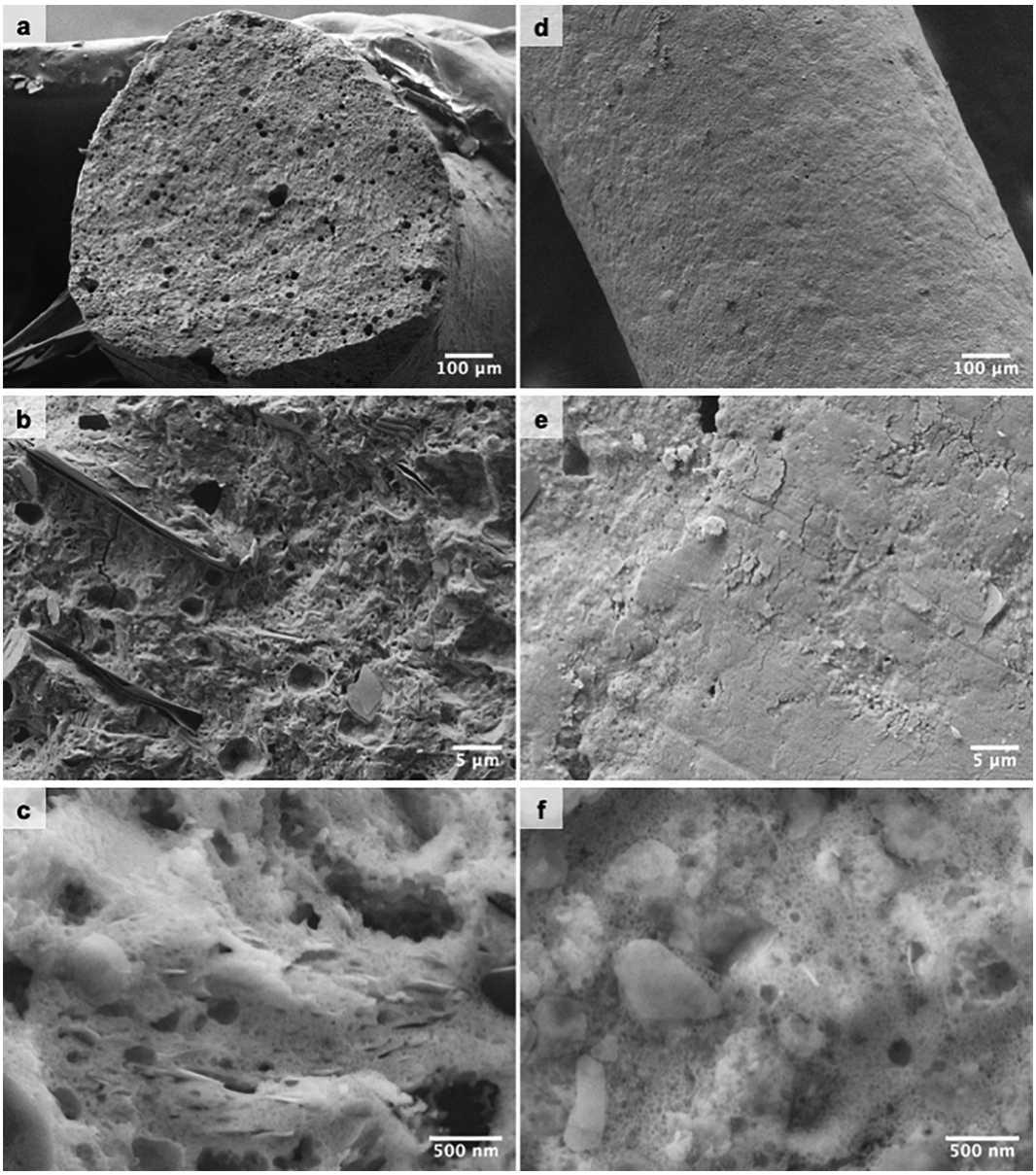

Fig. 2. SEM images of a printed lattice: a), b), c) filament section; d), e), f) filament surface at increasing magnification. Impurities are pointed with arrows.

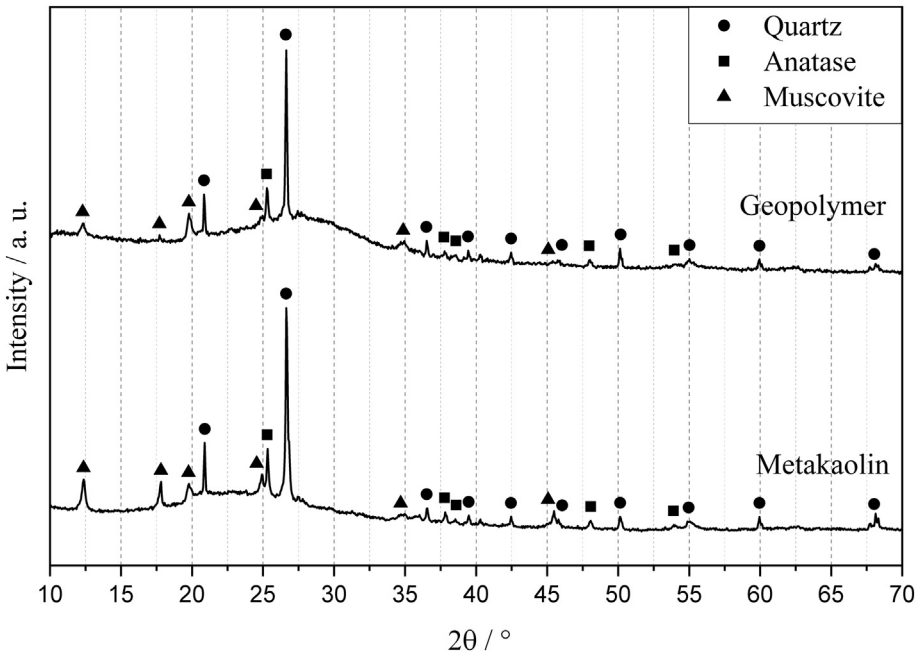

Fig. 3. XRD analysis on the consolidated geopolymer ink compared with the metakaolin raw material.

$$\ln q_c = \frac{B+1}{\beta \cdot \ln t} \tag{5}$$

The elemental composition of samples before and after ammonium ion exchange tests was determined semi-quantitatively with an X-ray fluorescence (XRF) spectrometer (Bruker AXS S4 Pioneer Billerica). Before the analysis, samples were ground to a fine powder, added with 6% C-wax as binder and compressed to tablets with diameter of 37 mm.

3. Results and discussion

Fig. 1 shows details of the disc shaped lattices fabricated via DIW. The optimization of the rheological properties of the ink and a good control over the processing parameters (pressure, flow rate and feed rate) allowed to deposit continuous filaments with regular diameters and to effectively follow the designed 0–45-90° sequential build-up of layers producing continuous yet tortuous channels.

After completion of the geopolymerization reaction, the sorbents had a diameter of 43.51 ± 0.73 mm and a height of 9.25 ± 0.46 mm, confirming the good repeatability of the fabrication procedure. Sections of the samples (Fig. 1c) show very limited deformation of the unsupported filaments and the presence of open channels in the Z direction, as designed.

The struts retained a circular shape, with a diameter of 0.77 ± 0.01 mm (corresponding to a linear shrinkage of ~10%, due to drying). Fig. 2 compares the inner microstructure of the filaments (a-c) and their surface (d-f), by means of SEM images. Some spherical pores with the dimension of a few microns can be detected inside the struts and are most probably caused by air bubbles entrapped in the ink during mixing and syringe filling. The surface of the struts appears generally denser than their core.

The amorphous geopolymer matrix looks homogeneous throughout the whole filament; the few platelet inclusions (see Fig. 2b, pointed with arrows) can be attributed to metakaolin impurities. At higher magnification, the typical mesoporous structure of geopolymers can be detected both inside the struts and on their surface; mesopores are the sites in which sorption and ion exchange take place [23].

XRD analyses were performed on the reacted geopolymer and on the metakaolin raw material to identify the impurities and determine the occurrence of the reaction. The results (Fig. 3) indicate that the metakaolin raw material contains quartz (SiO_2), anatase (TiO_2) and muscovite ($KAl_2(Si_3Al)O_{10}(OH)_2$) impurities (the latter are likely the ones detected with the SEM); metakaolin ($Al_2O_3 \cdot 2SiO_2$) itself is X-ray amorphous and produces only a broad hump centered at 20–25°. After the reaction, the maximum of the amorphous hump shifted to approximately 25–30°, indicating that a change happened in the chemical structure. No crystalline phases (zeolite-type structures) were formed during geopolymerization.

Physical analyses on the printed components revealed a bulk density of 0.95 ± 0.03 g/cm^3, apparent density of 1.86 ± 0.01 g/cm^3 and true density of 1.99 ± 0.01 g/cm^3. Table 1 reports the computed total, open and closed porosity values. The limited amount of closed porosity was also confirmed by image analysis on SEM images (see Fig. 2a). The open porosity matches well the theoretical porosity from design.

Table 1
Porosity of the printed components.

Value	[%vol]
Theoretical porosity (by design)	50.4
Total porosity	52.4 ± 1.5
Open porosity	49.3 ± 1.6
Closed porosity (relative to the struts)	6.5 ± 0.4

Table 2
Specific surface area and average pore size of the printed components at different stages and of powdered geopolymers.

	Specific surface area (BET)	Average pore size (BJH)
Printed structures	3.7 ± 0.5 m^2/g	22.0 nm
Printed structures after washing	12.2 ± 0.6 m^2/g	9.6 nm
Powders from PEG-free casts	18.3 ± 0.9 m^2/g	7.8 nm

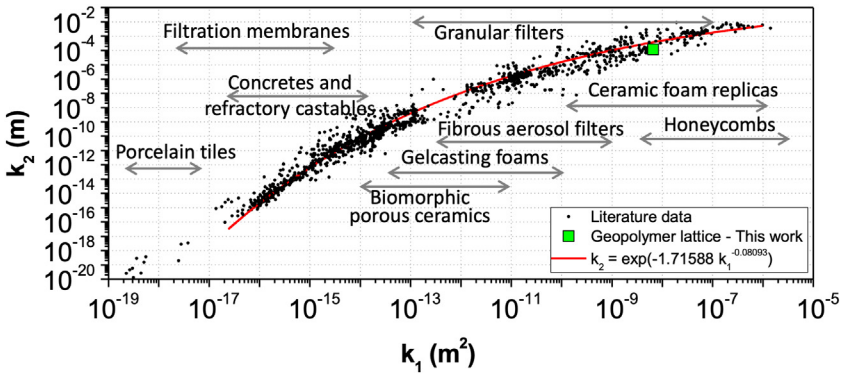

Fig. 4. Permeability map (adapted from Innocentini et al. [41]) comparing printed lattices and conventional porous ceramics.

Table 3
Comparison between the printed lattices and packed beds filled with GAC and PAC.

Packing material	k_1 (10^{-9} m^2)	k_2 (10^{-4} m)	d_p (mm)	ε (%)
Lattice	7.23	1.29	–	45
GAC	0.98	0.66	1.00	45
PAC	0.01	0.07	0.10	45

Tested under compression, the lattices showed a compressive strength of 6.0 ± 1.8 MPa; the value is in accordance with previous results obtained from components fabricated using the same ink [32]. Note that the compressive strength of such lattices does not only depend on the matrix properties and on the lattice porosity, but also on the build-up sequence: different orientations provide more or fewer nodes within the structure. Tests repeated on washed lattices showed no significant decrease (compressive strength of 4.7 ± 0.8 MPa). It can be stated that the washing procedure does not affect the mechanical strength of the lattices and that they can successfully withstand water pressure in pipes (usually ~$1 \cdot 10^5$ Pa – $5 \cdot 10^5$ Pa or 1–5 bar).

BET analysis reported a low SSA value for the printed structures (3.7 ± 0.4 m^2/g), which can be explained with the presence of PEG entrapped in the geopolymer matrix (meso-)pores, making them inaccessible. Table 2 compares the as prepared printed structures with those subject to the washing procedure, which showed rather higher SSA (12.2 ± 0.4 m^2/g). This indicates that PEG is effectively removed by the washing procedure, as confirmed by the FTIR spectra in the Supplementary Information. As a result, smaller pores became accessible and the average pore size decreased. Geopolymer powders obtained from PEG-free casts possessed similar pore size, yet a slightly higher SSA value (18.3 ± 0.9 m^2/g), which may indicate that some residual PEG was still present after the washing procedure. However, PEG would be entirely removed upon use in continuous flow.

The SSA value of the geopolymer powders was comparable to the one previously reported for the optimization of powdered Na-based geopolymer sorbents of similar compositions and close to the that of the one providing the highest NH_4^+ removal efficiency [23].

It should be noted that no linear correlation between SSA and NH_4^+ ion exchange capacity was detected in the previous work [23]. In fact, the same lack of correlation between specific surface area (detected by N_2 adsorption) and cation exchange capacity for clay mineral-containing soils have been reported [43]. Possible explanation for this behavior is that the N_2 gas is unable to penetrate interlayers of unexpanded clay minerals [43]. Indeed, the aluminosilicate network structure of geopolymers could also exhibit expansion, as it has been

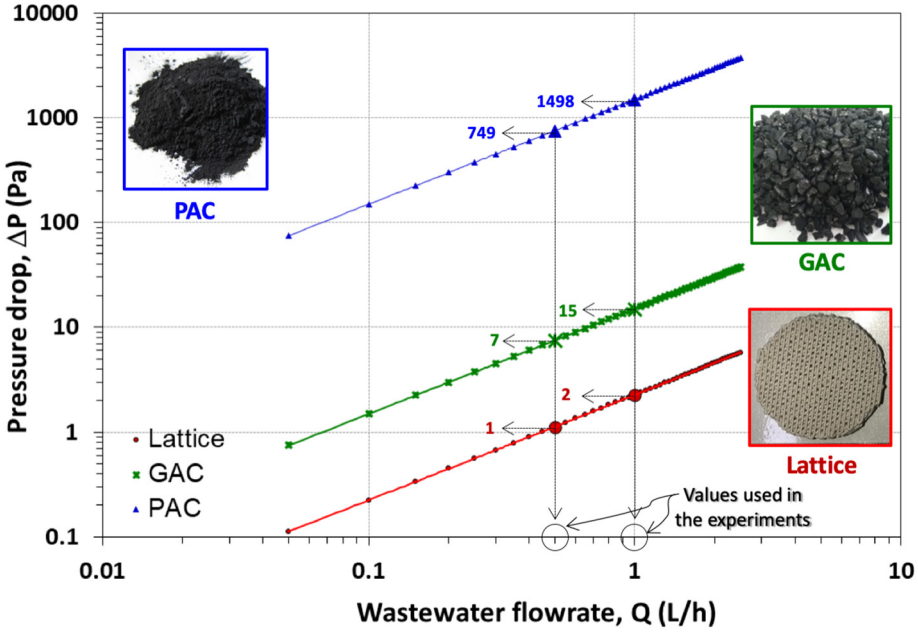

Fig. 5. Prediction of pressure drop during the flow of wastewater through the column used in the experiments containing different packing materials (GAC, PAC and a printed lattice).

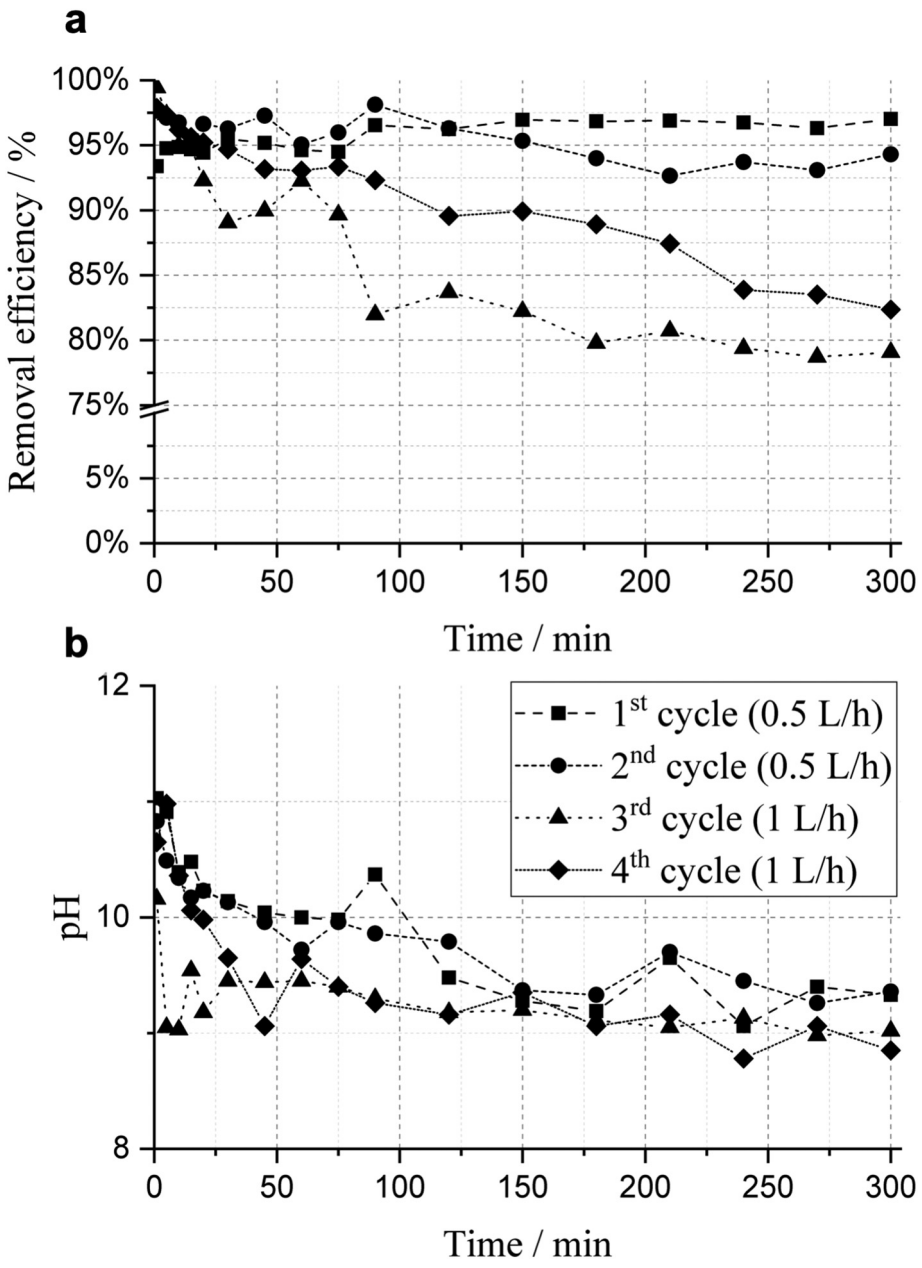

Fig. 6. a) The removal efficiency of NH_4^+ ions from the model solution for multiple cycles of 300 min and b) the pH of the treated water during the experiments. The inlet NH_4^+ concentration was 50 mg/L, pH was 7, and $T = 20$ °C. The contact time was either 19.3 min (0.5 L/h) or 9.6 min (1 L/h), which corresponded to 0.33 m/h or 0.66 m/h surface loading rates, respectively.

shown that the specific surface area increases after exchange of Na^+ to NH_4^+ [27]. Nevertheless, the average pore size has a clearer role in the ion exchange process: micro or mesopores should indeed be present for an efficient operation.

The parabolic relationship between pressure drop and superficial air velocity for two printed components (1 and 2) was confirmed by the permeability tests; experimental data are in good accordance with Forchheimer's equation (Eq. (1)) with a correlation coefficient $R^2 > 0.99$. The average permeability coefficients for the cylinder design were $k_1 = 7.23 \pm 1.18 \cdot 10^{-9}$ m^2 and $k_2 = 1.29 \pm 0.22 \cdot 10^{-4}$ m.

Geopolymer sorbents could be installed in pipes or column, where water is pumped through the lattice structure to interact with the active surface sites containing exchangeable cations (here, Na^+ ions). The contact time t is directly proportional to the reactor length L, which can be increased by stacking several lattices along the flow direction. The pressure drop should be linearly dependent upon to the thickness of the stack (as stated by Eq. (1)), and the permeability coefficients should not vary, as they are intrinsic properties of the material. Nevertheless, for non-stochastic materials such as lattices, the frictional pressure loss at the surface may be significant and contribute to the total pressure drop. The influence of the stacking length on the permeability of the produced lattice sorbents was experimentally assessed by measuring the pressure drop through two samples stacked along the air flow direction (1 + 2). Results indicate that surface effects were not significant for the printed lattices; the coefficients for the stacked samples were $k_1 = 6.60 \cdot 10^{-9}$ m^2 and $k_2 = 1.20 \cdot 10^{-4}$ m (both within the calculated standard deviation). This is a confirmation that even the first layers of the sorbents retain their shape after deposition, with limited deformation and without restraining the channel openings at the bottom side. It should be noted that, when performing DIW, the first layers in particular tend to deform (flatten) because of the contact with the flat solid printing surface as well as the weight of subsequent layers. Therefore,

special attention should be given, when engineering the ink rheology, to its yield stress value (~80 Pa in our case).

The advantage of describing the permeability of porous materials using the k_1 and k_2 parameters is that they are intrinsic properties of the pores (depending on their size, volume, morphology, interconnectivity, etc.) and therefore may be used to simulate the $\Delta P(v_s)$ profile for other fluids or flow conditions (such as water flow through a pipe). Moreover, they also allow to compare the permeability of the printed lattices with those of more conventional porous media (see Fig. 4). The structure printed in this work allows the components to perform similarly to honeycombs and ceramic foam replicas, but at the same time they have lower porosity and therefore higher mechanical properties than stochastic foams [44]).

Comparatively with other sorbent materials, the printed lattice is expected to present much lower pressure drop under the same operational conditions. As an example, in Table 3, the experimental permeability coefficients k_1 and k_2 of the printed lattice are compared with the predicted values for packed beds filled with granular activated carbon (GAC) and powdered activated carbon (PAC), two typical sorbents used for wastewater treatment. Values were estimated based on Ergun equation [41,45], with average particle sizes (d_p) of 1.0 mm for GAC and 0.1 mm for PAC, and a same bed porosity (ε) of 45% of the printed lattice.

Values in Table 3 were used to compare the expected pressure drop of wastewater flowing through the column in flow rates of 0.5 and 1.0 L/h, corresponding to fluxes of 329 and 658 L/h.m^2, respectively. Eq. (1) was used to predict the pressure drop through the cylindrical column with diameter of 44 mm and length of 99 mm. Properties of the wastewater were based on water at 20 °C (ρ = 997 kg/m^3 and $\mu = 8.9 \times 10^{-4}$ Pa.s). Simulated curves are given in Fig. 5.

As observed in Fig. 5, for the flow rates applied in this work (0.5 and 1 L/h), the printed lattice presents much lower resistance to flow (1–2 Pa) compared to GAC (14–28 Pa) and PAC (1392–2783 Pa).

The influence of the selected geopolymer composition on the NH_4^+ exchange was addressed based on former work [23]. A rather clear linear correlation was shown between the Na_2O concentration and NH_4^+ removal capacity, as it relates to the amounts of exchangeable cations in geopolymers. The ink used in this work had a Na_2O/SiO_2 ratio similar to the one providing the highest NH_4^+ removal efficiency (successfully tested in powder and granulated form in another study [22]).

In Fig. 6, the NH_4^+ removal results for several cycles are reported together with the pH of the treated water; they are in agreement with an earlier publication, in which the regeneration rate was observed to improve with successive cycles [21].

The cumulative adsorbed amount of NH_4^+ per cycle was 1.6 and 2.6 mg g−1 for 0.5 and 1 L/ h flow rates, respectively. Slightly lower adsorption amounts (~1.1 mg g−1) were reported earlier for metakaolin-geopolymer granules in similar kind of column experiments [21], demonstrating that the printed lattices have a higher ion-exchange capacity per unit mass due to improved permeability and macroporosity. Moreover, as can be seen from Fig. 6, the sorbent could be used for a much longer time than 300 min as there is no decline in the removal rate during the first cycle at all. Therefore, the cumulative adsorbed amounts observed in this time-scale do not represent the total ion-exchange capacity, and thus are not comparable to equilibrium capacities reported earlier (i.e., 18, 29, and 32 mg g^{-1} for raw municipal wastewater, primary-treated municipal wastewater, and synthetic wastewater, respectively [22]). The initial NH_4^+ was approximately 50 mg/ L, which is representative of typical municipal wastewater. After treatment with the sorbent, the NH_4^+ concentration was consistently <4 mg/ L (which is a typical guideline value for wastewater discharge) during the first and second cycle. In the third and fourth cycles, though, NH_4^+ was >4 mg/ L in the end of the cycles. Prior to the treatment, the pH was around 7 but after the treatment it increased up to 11 during the first minutes of the experiment. The lower initial pH in the 3rd cycle could be related to the sudden increase in water flow; however, it leveled out during the experiment. The pH settled between 9 and 9.5 towards the end of all experiments. It should be noted that NH_4^+ begins to volatilize as NH_3 at pH values larger than 9. However, previous study indicated that this volatilization is very minor (< 6% of total removal) up to pH 11 [22]. Therefore, in this study the volatilization of NH_3 should not play a major role. Consequently, the obtained results validate the suitability of 3D-printed metakaolin geopolymers for NH_4^+ removal and their regenerability.

Mass transfer in printed components during the column test was evaluated using the data from the 1st cycle. The natural logarithmic plot of cumulative adsorbed amount (q_c) versus time (t) results a straight line with a good fit: $R^2 > 0.999$ (Fig. 7a) allowing B and 1/β (i.e., potential mass transfer index and reciprocal of sorbate-sorbent affinity parameter, respectively) to be obtained reliably from the intercept and slope, respectively. Fig. 7b shows the external, internal and global mass transfer coefficients as a function of the percentage of outflow. As the printed geopolymer approach saturation, the mass transfer coefficients approach zero. The internal (i.e., pore) diffusion coefficient, $[kLa]_d$, has negative values and thus it can be concluded that the mass transfer resistance is dependent on internal diffusion [42]. This confirms the importance of a tailored porosity for effective NH_4^+ removal. Similar result was also obtained in the case of granulated metakaolin geopolymer in NH_4^+ ion exchange [22].

Table 4 reports the composition of the sorbents before the washing procedure and the ion exchange tests and after the 4th cycle (excluding traces and impurities). The sum of oxides constituent concentrations (SiO_2, Al_2O_3, Na_2O) was lower than 100%$_{wt}$ due to significant loss on ignition (LOI) reported during the analysis; this can be attributed to the release of PEG as well as of water (moisture and chemisorbed water) [46]. The amount of PEG accounted for 5%$_{wt}$; it was assumed to be flushed away after the washing procedure and ion exchange tests,

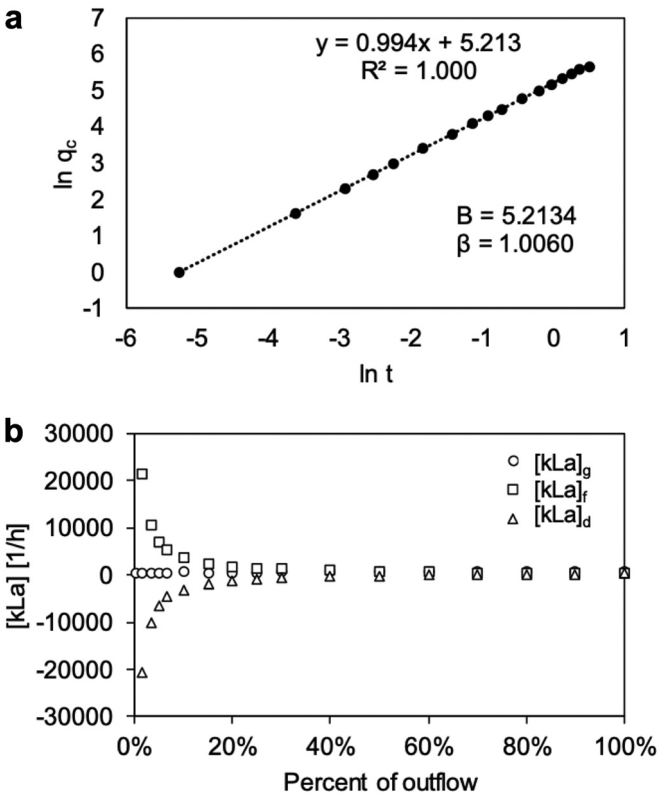

Fig. 7. a) Plot of ln q_c versus ln t and b) plot of $[k_La]_g$, $[k_La]_f$, and $[k_La]_d$ as a function of percentage of outflow. $[k_La]_d$, $[k_La]_f$, and $[k_La]_g$ are the internal, external, and global mass transfer coefficients and ln q_c and ln t are natural logarithms of the cumulative adsorbed amount of NH_4^+ and time, respectively.

Table 4
Composition ($\%_{wt}$ and molar ratios) of the samples before the washing procedure and the ion exchange tests and after the 4th cycle of the ion exchange tests.

	SiO_2 ($\%_{wt}$)	Al_2O_3 ($\%_{wt}$)	Na_2O ($\%_{wt}$)	LOI ($\%_{wt}$)	SiO_2/Al_2O_3 (mol/mol)	Na_2O/Al_2O_3 (mol/mol)	H_2O/Al_2O_3 (mol/mol)
Before	46.8	18.7	11.5	23.0	4.2	1.0	5.5
After	51.3	20.9	9.7	18.2	4.2	0.8	4.9

which was confirmed by a decrease in LOI of 4.8%$_{wt}$. If the remaining LOI is attributed to water, the H_2O/Al_2O_3 molar ratio in the samples is 5.5 and 4.9 before and after ion exchange, respectively; this result is in agreement with the stoichiometry of the geopolymerization reaction, indicating that the consolidated sorbents should retain chemisorbed water at a H_2O/Al_2O_3 molar ratio between 5 and 7 after the reaction occurred. The initial organic carbon content (due to the added PEG) of the printed disks after curing was approximately 0.032%$_{wt}$. If we assume that the disks are capable of treating minimum 179 L of synthetic effluent per kg of unit mass (from the data presented in Fig. 6), this means that, even by considering unwashed samples, the leached total organic carbon (TOC) would be less than 1.79 mg/L. The typical TOC values for municipal wastewater effluents after the final treatment steps are 5–15 mg/L. [47] Therefore, the leached TOC from filters is likely to decrease quickly as the filter is washed or used to a level that does not significantly contribute to the background values.

A decrease in the Na_2O content was detected after the initial washing and four ion-exchange-regeneration cycles (Table 4). A mass balance calculation reveals that the decrease of Na^+ was approximately 0.58 mol Na^+ per kg of sorbent, whereas the intake of NH_4^+ (in the 4th cycle) corresponded to 0.16 mol of NH_4^+ per kg of sorbent. Since the ion-exchange of Na^+ to NH_4^+ occurs in a 1:1 mole ratio, the difference in NH_4^+ intake and Na^+ decrease (i.e., 0.42 mol/kg) corresponds to the residual Na^+ removed during the initial washing.

4. Conclusions

The present study provides a proof of concept for the employment of porous geopolymer components fabricated via direct ink writing for the removal of NH_4^+ ions from wastewater.

Geopolymers have a high affinity for NH_4^+ as the charge-balancing Na^+ cations in the geopolymer aluminosilicate network can be effectively exchanged to NH_4^+. The combination of material and manufacturing process plays a major role in providing accessibility to the charge-bearing sites, as it allows to tailor the porosity of the sorbents on multiple levels and therefore their properties:

- (Ultra-)macroporosity (sub-millimeter range): the designed log-pile structure possessed continuous yet tortuous channels and a non-stochastic open (macro)porosity of 49.3 ± 1.6%$_{vol}$. As a result, the printed sorbents showed high permeability, low resistance to flow and sufficient compressive strength (6.0 ± 1.8 MPa) to withstand water pressure in pipes.
- Mesoporosity (2–50 nm range): the geopolymerization reaction results in the formation of a mesoporous network confirmed by high magnification SEM and by the SSA value (12.2 m^2/g) and average pore size (9.58 nm) measured for the printed sorbents after washing.

The printed geopolymer sorbents show high cation exchange capacity, with NH_4^+ removal efficiency ≥80% also after four cycles. No decline in the removal rate was detected during the first cycle. The 3D-printed geopolymers have ion-exchange capacity larger than 2.6 mg g^{-1}.

During the tests, the sorbents underwent very little compositional changes and maintained a high amount of active (Na^+) ions. Thanks to their high mechanical properties and permeability, they were not physically damaged during the ion exchange cycles, meaning that they could also be regenerated and reused several times.

To conclude, printed geopolymer sorbents provide for a very valid alternative to synthetic zeolites and conventional ceramics, due to the following reasons:

- their production is less energy intensive as they consolidate at low temperature;
- they could be prepared from locally available materials, including wastes (fly ashes, slags and so on);
- the synergy between material and fabrication process provides for effective tailoring and customization of sorbents with optimal porosity, permeability and mechanical properties.

Data availability

The raw and processed data required to reproduce these findings are available to download from http://urn.fi/urn:nbn:fi:att:f649e3f6-b027-4b64-bcd8-da983156363b

Declaration of Competing Interest

We wish to confirm that there are no known conflicts of interest associated with this publication and there has been no significant financial support for this work that could have influenced its outcome.

We confirm that the manuscript has been read and approved by all named authors and that there are no other persons who satisfied the criteria for authorship but are not listed. We further confirm that the order of authors listed in the manuscript has been approved by all of us.

We confirm that we have given due consideration to the protection of intellectual property associated with this work and that there are no impediments to publication, including the timing of publication, with respect to intellectual property. In so doing we confirm that we have followed the regulations of our institutions concerning intellectual property.

We understand that the Corresponding Author is the sole contact for the Editorial process (including Editorial Manager and direct communications with the office). He/she is responsible for communicating with the other authors about progress, submissions of revisions and final approval of proofs. We confirm that we have provided a current, correct email address which is accessible by the Corresponding Author and which has been configured to accept email from tero.luukkonen@oulu.fi

Acknowledgements

This work was supported by the Academy of Finland (grant #315103), by the China Scholarship Council (CSC, Grant # 201407565009) and by MIUR PRIN2017 (project # 2017PMR932).

The authors thank Imerys S.A. and Ingessil S.r.l. for kindly donating the raw materials.

Appendix A. Supplementary data

Supplementary data to this article can be found online at https://doi.org/10.1016/j.matdes.2020.109006.

References

[1] Y. Liu, C. Yan, Z. Zhang, H. Wang, S. Zhou, W. Zhou, A comparative study on fly ash, geopolymer and faujasite block for Pb removal from aqueous solution, Fuel. 185 (2016) 181–189, https://doi.org/10.1016/j.fuel.2016.07.116.

[2] P. Duan, C. Yan, W. Zhou, D. Ren, Development of fly ash and iron ore tailing based porous geopolymer for removal of Cu(II) from wastewater, Ceram. Int. 42 (2016) 13507–13518, https://doi.org/10.1016/j.ceramint.2016.05.143.

[3] M.N. Mužek, S. Svilović, M. Ugrina, J. Zelić, Removal of copper and cobalt ions by fly ash-based geopolymer from solutions-equilibrium study, Desalin. Water Treat. 57 (2016) 10689–10699, https://doi.org/10.1080/19443994.2015.1040077.

[4] Y. Ge, X. Cui, Y. Kong, Z. Li, Y. He, Q. Zhou, Porous geopolymeric spheres for removal of Cu(II) from aqueous solution: synthesis and evaluation, J. Hazard. Mater. 283 (2015) 244–251, https://doi.org/10.1016/j.jhazmat.2014.09.038.

[5] M.S. Al-Harahsheh, K. Al Zboon, L. Al-Makhadmeh, M. Hararah, M. Mahasneh, Fly ash based geopolymer for heavy metal removal: a case study on copper removal, J. Environ. Chem. Eng. 3 (2015) 1669–1677, https://doi.org/10.1016/j.jece.2015.06.005.

[6] M.I. Khan, T.K. Min, K. Azizli, S. Sufian, H. Ullah, Z. Man, Effective removal of methylene blue from water using phosphoric acid based geopolymers: synthesis, characterizations and adsorption studies, RSC Adv. 5 (2015) 61410–61420, https://doi.org/10.1039/c5ra08255b.

[7] H. Runtti, T. Luukkonen, M. Niskanen, S. Tuomikoski, T. Kangas, P. Tynjälä, E.T. Tolonen, M. Sarkkinen, K. Kemppainen, J. Rämö, U. Lassi, Sulphate removal over barium-modified blast-furnace-slag geopolymer, J. Hazard. Mater. 317 (2016) 373–384, https://doi.org/10.1016/j.jhazmat.2016.06.001.

[8] T. Luukkonen, H. Runtti, M. Niskanen, E.T. Tolonen, M. Sarkkinen, K. Kemppainen, J. Rämö, U. Lassi, Simultaneous removal of Ni(II), as(III), and Sb(III) from spiked mine effluent with metakaolin and blast-furnace-slag geopolymers, J. Environ. Manag. 166 (2016) 579–588, https://doi.org/10.1016/j.jenvman.2015.11.007.

[9] C. Bai, G. Franchin, H. Elsayed, A. Zaggia, L. Conte, H. Li, P. Colombo, High-porosity geopolymer foams with tailored porosity for thermal insulation and wastewater treatment, J. Mater. Res. 32 (2017)https://doi.org/10.1557/jmr.2017.127.

[10] C. Min Li, Y. He, Q. Tang, K. Tuo Wang, X. Min Cui, C. Min Li, Y. He, Q. Tang, K. Tuo Wang, X. Min Cui, Study of the preparation of CdS on the surface of geopolymer spheres and photocatalyst performance, Mater. Chem. Phys. 178 (2016) 204–210, https://doi.org/10.1016/j.matchemphys.2016.05.013.

[11] J.R. Gasca-Tirado, A. Manzano-Ramírez, P.A. Vazquez-Landaverde, E.I. Herrera-Díaz, M.E. Rodríguez-Ugarte, J.C. Rubio-Ávalos, V. Amigó-Borrás, M. Chávez-Páez, Ion-exchanged geopolymer for photocatalytic degradation of a volatile organic compound, Mater. Lett. 134 (2014) 222–224, https://doi.org/10.1016/j.matlet.2014.07.090.

[12] Y. Ge, Y. Yuan, K. Wang, Y. He, X. Cui, Preparation of geopolymer-based inorganic membrane for removing Ni2+ from wastewater, J. Hazard. Mater. 299 (2015) 711–718, https://doi.org/10.1016/j.jhazmat.2015.08.006.

[13] M. Xue Xu, Y. He, C. Qun Wang, X. Feng He, X. Qing He, J. Liu, X. Min Cui, M. Xue Xu, Y. He, C. Qun Wang, X. Qing Feng, X. Qing He, Feng He, J. Liu, X. Min Cui, Preparation and characterization of a self-supporting inorganic membrane based on metakaolin-based geopolymers, Appl. Clay Sci. 115 (2015) 254–259, https://doi.org/10.1016/j.clay.2015.03.019.

[14] G. Bumanis, D. Bajare, The effect of porous alkali activated material composition on buffer capacity in bioreactors, Int. J. Chem. Nucl. Metall. Mater. Eng. 8 (2014) 1040–1046.

[15] G. Bumanis, K. Rugele, D. Bajare, The effect of alkaline material particle size on adjustment ability of buffer capacity, Medziagotyra. 21 (2015) 405–409, https://doi.org/10.5755/j01.ms.21.3.7325.

[16] G. Ascensão, M.P. Seabra, J.B. Aguiar, J.A. Labrincha, Red mud-based geopolymers with tailored alkali diffusion properties and pH buffering ability, J. Clean. Prod. 148 (2017) 23–30, https://doi.org/10.1016/j.jclepro.2017.01.150.

[17] R.M. Novais, M.P. Seabra, J.A. Labrincha, Porous geopolymer spheres as novel pH buffering materials, J. Clean. Prod. 143 (2017) 1114–1122, https://doi.org/10.1016/j.jclepro.2016.12.008.

[18] R.M. Novais, T. Gameiro, J. Carvalheiras, M.P. Seabra, L.A.C. Tarelho, J.A. Labrincha, I. Capela, High pH buffer capacity biomass fly ash-based geopolymer spheres to boost methane yield in anaerobic digestion, J. Clean. Prod. 178 (2018) 258–267, https://doi.org/10.1016/j.jclepro.2018.01.033.

[19] S. Horpibulsuk, C. Suksiripattanapong, W. Samingthong, R. Rachan, A. Arulrajah, Durability against wetting-drying cycles of water treatment sludge-fly ash geopolymer and water treatment sludge-cement and silty clay-cement systems, J. Mater. Civ. Eng. 28 (2016) 1–9, https://doi.org/10.1061/(ASCE)MT.1943-5533.0001351.

[20] C. Bai, P. Colombo, Processing, properties and applications of highly porous geopolymers: a review, Ceram. Int. 44 (2018) 16103–16118, https://doi.org/10.1016/j.ceramint.2018.05.219.

[21] T. Luukkonen, M. Sarkkinen, K. Kemppainen, J. Rämö, U. Lassi, Metakaolin geopolymer characterization and application for ammonium removal from model solutions and landfill leachate, Appl. Clay Sci. (2016)https://doi.org/10.1016/j.clay.2015.10.027.

[22] T. Luukkonen, K. Věžníková, E.T. Tolonen, H. Runtti, J. Yliniemi, T. Hu, K. Kemppainen, U. Lassi, Removal of ammonium from municipal wastewater with powdered and granulated metakaolin geopolymer, Environ. Technol. (United Kingdom). 39 (2018) 414–423, https://doi.org/10.1080/09593330.2017.1301572.

[23] T. Luukkonen, E.T. Tolonen, H. Runtti, K. Kemppainen, P. Perämäki, J. Rämö, U. Lassi, Optimization of the metakaolin geopolymer preparation for maximized ammonium adsorption capacity, J. Mater. Sci. 52 (2017) 9363–9376, https://doi.org/10.1007/s10853-017-1156-9.

[24] R.G. Wetzel, Limnology: Lake and River Ecosystems, 3rd Editio, Elsevier, San Diego (CA), 2001.

[25] J.H. Hwang, J.A. Oleszkiewicz, Effect of cold-temperature shock on nitrification, Water Environ. Res. 79 (2007) 964–968, https://doi.org/10.2175/106143007x176022.

[26] Y. Lin, M. Guo, N. Shah, D.C. Stuckey, Economic and environmental evaluation of nitrogen removal and recovery methods from wastewater, Bioresour. Technol. 215 (2016) 227–238, https://doi.org/10.1016/j.biortech.2016.03.064.

[27] J.R. Gasca-Tirado, A. Manzano-Ramírez, E.M. RiveraMuñoz, R. Velázquez-Castillo, M. Apátiga-Castro, R. Nava, A. Rodríguez-López, Ion exchange in Geopolymers, New Trends Ion Exch. Stud., IntechOpen 2018, pp. 71–82, https://doi.org/10.5772/intechopen.80970.

[28] ISO/ASTM International 2015, Additive manufacturing — General principles — Terminology, 2015 1–19, https://doi.org/10.1520/ISOASTM52900-15.

[29] A. Zocca, G. Franchin, P. Colombo, J.B.T.-R.M. in M.S, M.E. Günster, Additive manufacturing, ref, Modul. Mater. Sci. Mater. Eng. (2020) 1–19, https://doi.org/10.1016/B978-0-12-803581-8.12081-8.

[30] M. Xia, J.G. Sanjayan, J.G. Sanjayan, Method of formulating geopolymer for 3D printing for construction applications, Mater. Des. 110 (2016) 382–390, https://doi.org/10.1016/j.matdes.2016.07.136.

[31] M. Romagnoli, C. Leonelli, E. Kamse, M. Lassinantti Gualtieri, Rheology of geopolymer by DOE approach, Constr. Build. Mater. 36 (2012) 251–258, https://doi.org/10.1016/j.conbuildmat.2012.04.122.

[32] G. Franchin, P. Scanferla, L. Zeffiro, H. Elsayed, A. Baliello, G. Giacomello, M. Pasetto, P. Colombo, Direct ink writing of geopolymeric inks, J. Eur. Ceram. Soc. 37 (2017) https://doi.org/10.1016/j.jeurceramsoc.2017.01.030.

[33] J. Zhong, G.X. Zhou, P.G. He, Z.H. Yang, D.C. Jia, 3D printing strong and conductive geo-polymer nanocomposite structures modified by graphene oxide, Carbon N. Y. 117 (2017) 421–426, https://doi.org/10.1016/j.carbon.2017.02.102.

[34] T. Luukkonen, J. Yliniemi, H. Sreenivasan, K. Ohenoja, M. Finnilä, G. Franchin, P. Colombo, Ag- or Cu-modified geopolymer filters for water treatment manufactured by 3D printing, direct foaming, or granulation, Sci. Rep. 10 (2020) 1–14, https://doi.org/10.1038/s41598-020-64228-5.

[35] B. Panda, S.C. Paul, L.J. Hui, Y. Wei, D. Tay, M. Jen, Y.W.D. Tay, M.J. Tan, Y. Wei, D. Tay, M. Jen, Y.W.D. Tay, M.J. Tan, Additive manufacturing of geopolymer for sustainable built environment, J. Clean. Prod. 167 (2018) 281–288, https://doi.org/10.1016/j.jclepro.2017.08.165.

[36] S.H. Bong, B. Nematollahi, A. Nazari, M. Xia, J. Sanjayan, Method of optimisation for ambient temperature cured sustainable geopolymers for 3D printing construction applications, Materials (Basel). 16 (2019)https://doi.org/10.3390/ma12060902.

[37] S. Al-Qutaifi, A. Nazari, A. Bagheri, Mechanical properties of layered geopolymer structures applicable in concrete 3D-printing, Constr. Build. Mater. 176 (2018) 690–699, https://doi.org/10.1016/j.conbuildmat.2018.04.195.

[38] A. Zocca, P. Colombo, C.M. Gomes, J. Guenster, Additive manufacturing of ceramics: issues, potentialities and opportunities, J. Am. Ceram. Soc. 98 (2015) 1983–2001.

[39] B.H. Mo, H. Zhu, X.M. Cui, Y. He, S.Y. Gong, Effect of curing temperature on geopolymerization of metakaolin-based geopolymers, Appl. Clay Sci. 99 (2014) 144–148, https://doi.org/10.1016/j.clay.2014.06.024.

[40] S. Gražulis, A. Daškevič, A. Merkys, D. Chateigner, L. Lutterotti, M. Quirós, N.R. Serebryanaya, P. Moeck, R.T. Downs, A. Le Bail, Crystallography open database (COD): an open-access collection of crystal structures and platform for world-wide collaboration, Nucleic Acids Res. 40 (2012) D420–D427, https://doi.org/10.1093/nar/gkr900.

[41] M.D.M.M. Innocentini, P. Sepulveda, F.S. dos Ortega, Permeability, Cell. Ceram. Struct. Manuf. Prop. Appl, Wiley-VCH, Weinheim 2005, pp. 313–341, https://doi.org/10.1002/3527606696.

[42] M.A. Fulazzaky, M.H. Khamidun, R. Omar, Understanding of mass transfer resistance for the adsorption of solute onto porous material from the modified mass transfer factor models, Chem. Eng. J. 228 (2013) 1023–1029, https://doi.org/10.1016/j.cej.2013.05.100.

[43] Y. Yukselen, A. Kaya, Prediction of cation exchange capacity from soil index properties, Clay Miner. 41 (2006) 827–837, https://doi.org/10.1180/0009855064140222.

[44] R. Rice, Mechanical properties, Cell. Ceram. Struct. Manuf. Prop. Appl, Wiley-VCH, Weinheim 2005, pp. 291–312, https://doi.org/10.1002/3527606696.

[45] S. Ergun, Fluid flow through packed columns, Chem. Eng. Prog. 48 (1952) 89–94.

[46] B.-S. King, D. Vivit, Loss-on-ignition corrections in the XRF analysis of silicate rocks, X-Ray Spectrom. 17 (1988) 145–147, https://doi.org/10.1002/xrs.1300170406.

[47] D. Dubber, N.F. Gray, Replacement of chemical oxygen demand (COD) with total organic carbon (TOC) for monitoring wastewater treatment performance to minimize disposal of toxic analytical waste, J. Environ. Sci. Heal. A. 45 (2010) 1595–1600, https://doi.org/10.1080/10934529.2010.506116.